BII-8

Micro-plasticity of uranium dioxide at room temperature

N. Igata[1], R.R. Hasiguti[1] and K. Domoto[2]

Abstract

Uranium dioxide has been considered to be a brittle material. In the present investigation the micro-plastic deformation was observed in the pre-fracture process of uranium dioxide at room temperature by means of strain rate dependence of flow stresses, ultrasonic measurements and etch pit techniques, using fused single crystals and sintered pellets. The difference between the ultrasonic attenuation of compressed state and that of annealed state shows the maximum as measured as a function of frequency. This is interpreted to be the resonance damping of dislocations introduced by plastic compression. The frictional force of dislocation movement is obtained from the decrement of over-damped region. The value is $\sim 3\times10^{-2}$ in sintered pellets and $\sim 1\times10^{-3}$ in fused single crystals.

§1. Introduction

Uranium dioxide has been considered to be a brittle material at room temperature and its plastic behavior has been studied only at high temperatures.

Scott, Hall and Williams(1) have discussed the effects of excess oxygen to high temperature plasticity, and they observed the plastic deformation at 1650°C in stoichiometric uranium dioxide, but were unable to detect any deformation at 1000°C. Rapperport and Huntress(2) have studied the deformation of single crystal in compression from 700 to 1900°C and observed the slip pattern, the most active slip plane being {100}. The results of Armstrong, Irvine and Martinson(3) concern the high temperature creep deformation in the temperature range from 1250 to 1400°C. At room

1 Department of Metallurgy, Faculty of Engineering, University of Tokyo, Bunkyo-ku, Tokyo.

2 Atomic Fuel Corporation, Tokai-mura, Ibaragi-ken.

temperature, however, only fracture strengths were reported in bending[4]–[7] and compression[5]–[8] and also it was recognized that the fracture is intercrystalline (9). It would be important in understanding the fracture mechanism of uranium dioxide to study its pre-fracture process and to know whether it can be plastically deformed or not. In this investigation, using fused UO_2 single crystals and sintered pellets the stress strain curve in compression test is investigated. The microplasticity in pre-fracture process at room temperature is found by strain rate sensitivity of flow stress, ultrasonic attenuation measurement and also the increase of etch pit density after compression. From the modulus and attenuation measurement the frictional force of dislocation movement was obtained and the mobility of dislocations is discussed.[3]

§ 2. Experimental procedure

(a) Specimen

The specimens are fused UO_2 single crystals made at Hanford Laboratory, U.S.A. and sintered UO_2 pellets made in Sumitomo Denkō Co. Japan. Their spectrographic analyses and specimen sizes are shown in Table I and II. Grain sizes in sintered pellets are controlled by annealing temperatures.

(b) Compression test

The compression tests were performed using a 10 ton universal testing machine. The loading rates were controlled at 37.5 kg/min in fused single crystals and at 100 ~ 1000 kg/min in sintered pellets within a few percents. In order to eliminate the friction effect of the specimen surfaces, teflon sheets were used but the effect was not detectable. The longitudinal strain was measured with wire strain guages which are attached to two opposite sides, their accuracy being 10^{-6}. The compression tests were performed at various loading rates, temperatures and grain sizes.

(c) Modulus and attenuation measurement

In modulus and attenuation measurements, the pulse echo

[3] Daniel and Takahashi also found the micro-plasticity of uranium dioxide at room temperature (22).

method is applied, using "Ultrasonic Comparator". A quartz crystal is attached with sarol or "Nonac" silicone grease.

The longitudinal or shear sound waves are transfered through the quartz crystal and the multi-pulse echoes are detected with the same crystal. The sound velocity is measured from the time interval of the multi-reflected echoes, and the attenuation a is measured from the exponential decay curve of the multi-reflected echoes. The elastic constants are obtained from the sound velocity using the following equations.

For a single crystal of [110] direction
$$\rho V_\ell^2 = \frac{1}{2}(C_{11} + C_{12} + 2C_{44}), \quad \text{----- (1)}$$

$$\rho V_\ell^2 = C_{44}, \quad \text{(Shear direction [001])}$$

$$\rho V_\ell^2 = \frac{1}{2}(C_{11} - C_{12}). \quad \text{(Shear direction [110])}$$

For a single crystal of [100] direction
$$\rho V_t^2 = C_{11}, \quad \text{---------- (2)}$$

$$= C_{44}, \quad \text{(Shear direction [010] or [001])}$$

For polycrystals
$$E = V_\ell^2 \rho \, \frac{(1+\sigma)(1-2\sigma)}{(1-\sigma)}, \quad \text{---------- (3)}$$

$$\mu = V_t^2 \rho = \frac{E}{2(1+\sigma)},$$

where V_ℓ and V_t are the velocities of longitudinal and shear waves, respectively, σ is the Poisson's ratio and ρ is the density. The decrement $\triangle$ is derived as follows.

$$\triangle = a\lambda \quad \text{---------- (4)}$$

$$a = \frac{1}{2(m-n)} \ell n \frac{A_n}{A_m} \ \text{cm}^{-1},$$

where λ is the wave length, A_n and A_m are the pulse heights of the n th and m th reflected waves, respectively.

(d) Etch pit technique

Specimens are polished with emery papers and then polished with diamond paste of 1/4 μ particle. The etching reagent is 1 part H_2SO_4 and 1 part H_2O_2 solution.(11)(12) The etching is performed by immersing the specimen for 5 min. at room temperature.

§3. Experimental results

(a) Compression test

The stress strain curves are obtained at various loading rates, grain sizes and testing temperatures. Some of the results are shown in Fig. 1. As the loading rate is constant, the strain rate is calculated from the stress strain curve. The flow stresses at the strains 1×10^{-3} and 2×10^{-3} are plotted against the strain rates in Fig. 2. The same stresses also plotted against the testing temperatures and the grain sizes are shown in Figs. 3 and 4. The strain rate sensitivities are expressed by the following equations:

$$\dot{\varepsilon} = 9.96 \times 10^{-56} \sigma^{5.25} \quad \text{at } \varepsilon = 1 \times 10^{-3},$$

$$\dot{\varepsilon} = 3.57 \times 10^{-84} \sigma^{8.03} \quad \text{at } \varepsilon = 2 \times 10^{-3}, \qquad \text{--------- (5)}$$

where σ is expressed in dyne/cm^2.

The flow stress increases with the testing temperature. The grain size dependence of flow stress does not show the $d^{-\frac{1}{2}}$ rule and the flow stress increases and decreases with the grain size. This behavior is different from ordinary metals and other oxides.

The fracture stress is also observed. The results are shown in Table III. These values agree fairly with the results of Burdick and Parker.(5)

(b) Modulus and attenuation measurements

The elastic constants of fused single crystals and sintered pellets are obtained from the sound velocity measurements using Eqs. (1) (2) and (3). The results are shown in Table IV. These values agree fairly well with the data of other investigators.(13)(14) The attenuation is measured before and after the compression in the frequency range of 5 Mc/s ~ 35 Mc/s. Since the obtained values include many factors which come from the measurement system, the size effect, etc., the differential decrements are taken. The results of fused single crystals and sintered pellets are shown in Fig. 5 and Fig. 6. In both figures, the decrement maxima are observed. This decrement maxima are not due to any relaxation, because the temperature dependence of the decrement at 5 Mc in the temperature range between -100°C +100°C shows no relaxation peak both before and after compression. As other origins are excluded from the frequency dependence, they are interpreted to be due to the resonance of dislocations(10) introduced by compression. This shows the increased dislocation density, and the micro-plasticity is evidently detected.

(c) Etch pits

The existence of micro-plasticity in the prefracture process of uranium dioxide is also supported by the increase of etch pits.

Since the etch pits are considered to be the dislocation pits,(11) the increase of pit density after compression shows the micro-plasticity. The dislocation densities obtained from the pit densities at various stress levels are shown in Fig. 7.

The dislocation density after compression is expressed roughly with the next equation.

$$n = 6.72 \times \sigma^{0.735}[4]$$

$$(2.5\times10^9 \text{ dynes/cm}^2 < \sigma < 8.0\times10^9 \text{ dynes/cm}^2) \text{ ----- (6)}$$

where σ is the applied compressive stress in dyne/cm^2 and

[4] This equation is only used in the stressed state.

n is the dislocation density per cm^2.

§4. Discussions

(a) Evidence for the micro-plasticity in prefracture process

As mentioned in the previous section, the evidence for the micro-plasticity in prefracture process of uranium dioxide at room temperature is confirmed with the strain rate sensitivity of the flow stress, the decrement maximum which is due to the resonance damping of dislocations increased with stress, and the increase of the etch pit density after stressing.

(b) Frictional force of dislocations

According to Granato-Lücke theory[15], the resonance damping of dislocations is expressed by the following equation.

$$\triangle_1 = \Omega \triangle_0 NL^2 \frac{\omega\tau}{1+\omega^2\tau^2} \qquad \text{---------- (7)}$$

where Ω is the orientation factor, $\triangle_0$ is the material constant, N is the dislocation density, L is the dislocation loop length, ω is the applied frequency and τ is the constant which is proportional to L^2 and the frictional force of dislocations B. Eq. (7) is well fitted to the experimental results of Figs. 5 and 6. In both figures, the curved lines show the theorical value assuming that the distribution of dislocation loop lengths is represented by the delta function. The value of B is obtained from the asymptote of the overdamped region using the dislocation densities obtained from the etch pit densities.[16] The dislocation loop length L is also calculated from the decrement maximum frequency using Eq. (7). The values of B and the dislocation loop lengths are shown in Table V. In the sintered pellets the values of B are higher than those of the fused single crystals. This would be partly due to the orientation factors of the pellets which are here assumed constant, and partly due to the excess oxygen. The latter origin may be justified, because the value of B shows a higher value in the irradiated LiF than in the unirradiated one[16]. In the fused single crystal the value of B is a little larger than that of KCl and almost the same as that of LiF[16].

Now, according to Johnston and Gilman[17] the plastic strain rate $\dot{\epsilon}$ is expressed as follows.

$$\dot{\epsilon} = n\, b\, v$$
$$v = \left(\frac{\sigma}{\sigma^*}\right)^m \qquad \text{---------- (8)}$$

where n is the dislocation density, b is the Burger's vector, v is the dislocation velocity, and σ^* and m are the constants. From Eq. (8),

$$\frac{\partial \log \dot{\epsilon}}{\partial \log \sigma} = \frac{\partial \log n}{\partial \log \sigma} + \frac{\partial \log v}{\partial \log \sigma} \qquad \text{---------- (9)}$$

Put the experimental values of Eqs. (5) and (6) into Eq. (9), assuming that the total strain rate is nearly equal to the plastic strain rate.

Then the following relation is derived.

$$\frac{\partial \log v}{\partial \log \sigma} = \begin{matrix} 4.52 & \text{at } \epsilon = 1\times10^{-3} \\ 7.30 & \text{at } \epsilon = 2\times10^{-3}. \end{matrix} \qquad \text{---------- (10)}$$

From Eqs. (5), (6) and (10), putting $b = 3.9\times10^{-8}$ cm,

$$v = \left(\frac{\sigma}{4.20 \times 10^{10}}\right)^{4.52} \qquad \text{at } \epsilon = 1\times10^{-3}$$

$$v = \left(\frac{\sigma}{3.38 \times 10^{10}}\right)^{7.30} \qquad \text{at } \epsilon = 2\times10^{-3} \qquad \text{---------- (11)}$$

These values of the exponent m are much lower than the value estimated from the experimental results of copper and near that of tungsten.[18] [19]

If we use the value of B, the mobility of dislocations must be expressed as follows.

$$v = \sigma B^{-1} \qquad \text{---------- (12)}$$

Comparing Eq. (11) with Eq. (12), it is found that the dislo-

cation mobility v is much lower in the former than in the latter at the same stress level. This would show that the frictional force of dislocations is much lower in the short range movement but becomes higher in the long range movement such as in the compression test.

The fracture mechanism of uranium dioxide at room temperature is not yet understood, but the dislocation behavior would be very important in crack nucleation and crack propagation, because the micro-plasticity is detected, and the Griffith crack lengths(20) calculated from Table III, assuming that the energy of the fracture surface is 1030 erg/cm²(21), are 0.27μ in the sintered pellets and 0.12μ in the fused single crystal which are much smaller than the grain sizes or the crystal size. The slip intersection would be one possible fracture mechanism.

§ 5. Summaries

(i) In the pre-fracture process of uranium dioxide at room temperature, the micro-plasticity is detected as follows.

a) The stress strain curve shows strain rate sensitivity.

b) From the differential decrement, the resonance damping of dislocations introduced by stress is observed.

c) After compression, the increase of etch pits is observed.

(ii) The frictional force of dislocations is lower in the fused single crystals than in the sintered pellets, the former being comparable with that of LiF. The higher value of B in the sintered pellets would be partly due to the assumed orientation factors and partly due to the excess oxygen. The frictional force of dislocations is also analysed from the strain rate sensitivity of the flow stress and compared with that obtained from the attenuation measurements.

References

(1) R. Scott, A.R. Hall and J. Williams, J. Nucl. Mat. 1, 39 (1959).

(2) E.J. Rapperport and A.M. Huntress, Nuclear Metals, Inc. Report NMI 1242 (1960).

(3) W.M. Armstrong, W.R. Irvine and R.H. Martinson, J. Nucl. Mat. 7, 133 (1962).

(4) W.A. Lamberston and J.H. Handwerk, ANL-5053 (1956).

(5) M.D. Burdick and H.S. Parker, J. Amer. Ceram. Soc. 39, 181 (1956).

(6) F.P. Knudsen, H.S. Parker and M.D. Burdick, J. Amer. Ceram. Soc. 43, 641 (1960)

(7) F.I. Peters, Corning Glass Works, R-1068, 1956.

(8) D.J. Bowers, W.A. Hedden, M.J. Snyder and W.H. Duckworth, BMI-1117, 1956.

(9) J. Belle, Proc. of the 2nd United Nations International Conf. on the Peaceful Uses of Atomic Energy, Geneva, 6, 585 (1958).

(10) R.R. Hasiguti, N. Igata and K. Domoto, Symposium on Non-destructive Testing in Nuclear Technology, SM 63/16, Bucharest, Romania, 1965.

(11) A. Briggs, Trans. Brit. Cer. Soc., 60, 505 (1961); also in AERE-M-859.

(12) T. Amanuma, K. Sakamoto, Tokenho, No.38 (1964), Atomic Fuel Corporation, Japan.

(13) J.B. Wachtman Jr., M.L. Wheat, H.J. Anderson and J.L. Bates, J. Nucl. Mat., 16, 39 (1965).

(14) S.M. Lang, U.S. Nat. Bur. Standards Monograph 6, 1960.

(15) A. Granato and K. Lücke, J. Appl. Phys. 27, 583, 789 (1956).

(16) T. Suzuki, A. Ikushima and M. Aoki, Acta Met. 12, 1231 (1964).

(17) W.G. Johnston and J.J. Gilman, J. Appl. Phys. 30, 129 (1959).

(18) R.P. Carreker, Jr. and W.R. Hibbard, Jr., Acta Met. 1, 654, (1953).

(19) G.T. Hahn, Acta Met., 10, 727 (1962).

(20) A.A. Griffith, Phil. Trans. Roy. Soc. 221, 163 (1920).

(21) G.C. Benson, P.I. Freeman and E. Dempsey, J. Amer. Cer. Soc. 46, 43 (1963).

(22) J.L. Daniel and S. Takahashi, to be published in Proc. International Conference on Fracture, 1965.

Table I. Spectrographic analysis (ppm)

	Ag	Al	Cd	Co	Cr	Cu	Fe	Mg	Mn
Fused single crystal	-	~10	-	-	-	-	~15	-	-
Sintered pellet	<0.2	48	<0.2	<5	<8	<3	<10	4	3

Ni	Si	V	Zn	Ca	F	Cl	C	N	B	O/U	density
-	~15	<50	<50	-	<2	<20	44	50	-	2.001	10.94
<10	10	<10	<50	10	<5	-	-	7	0.13	2.016	10.55

Table II. Specimen size

	dia.mm	length mm
Fused single crystal	4.80	No.1 4.735, No.2 4.760, No.3 4.683, No.4 4.758
Sintered pellet	12.50	10.30

Table III. Fracture strengths of three sintered pellets and a fused single crystal.

Material	Grain size	Fracture strength
Sintered pellets	6 μ	101 kg/mm^2
	"	96.0 kg/mm^2
	"	100 kg/mm^2
Fused single crystal	-	69.8 kg/mm^2 Direction of compression: [110]

Table IV. Elastic constants of fused single crystals and sintered pellets (in 10^{11} dynes/cm^2)

	C_{11}	C_{12}	C_{44}	$A = \frac{2C_{44}}{C_{11} - C_{12}}$
No.1	38.43	12.87	5.262	0.41
No.2	36.47	13.79	5.954	0.50
No.3	37.85	13.03	5.903	0.48
No.4	37.73		5.832	

E	Poisson's ratio	μ
19.56	0.312	7.459

Table V. Frictional force of dislocations and dislocation loop lengths obtained from the attenuation measurements

	Compression stress kg/mm^2	Dislocation density(from etch pits)cm^{-2}	Dislocation loop length L cm^2	Frictional force B dyne sec/cm^2
Sintered pellets	40.6	1.5×10^7	1.3×10^{-4}	1.4×10^{-2}
	28.5	3.9×10^7	0.70×10^{-4}	3.1×10^{-2}
	52.8	7.8×10^7	0.83×10^{-4}	2.2×10^{-2}
	73.2	6.5×10^7	1.0×10^{-4}	1.5×10^{-2}
Fused single crystals	10.0	2.2×10^6	3.8×10^{-4}	0.96×10^{-3} (at 33°C)
	10.0	2.2×10^6	4.0×10^{-4}	1.0×10^{-3} (at 100°C)

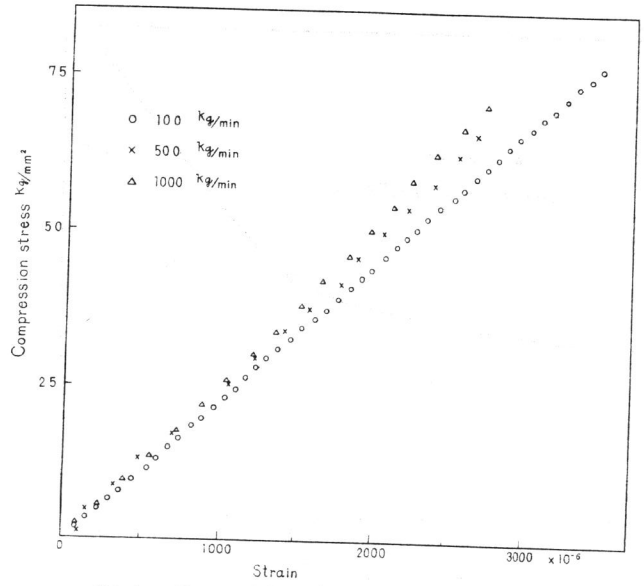

Fig. 1. Stress-strain curves of sintered pellets at various loading rates.

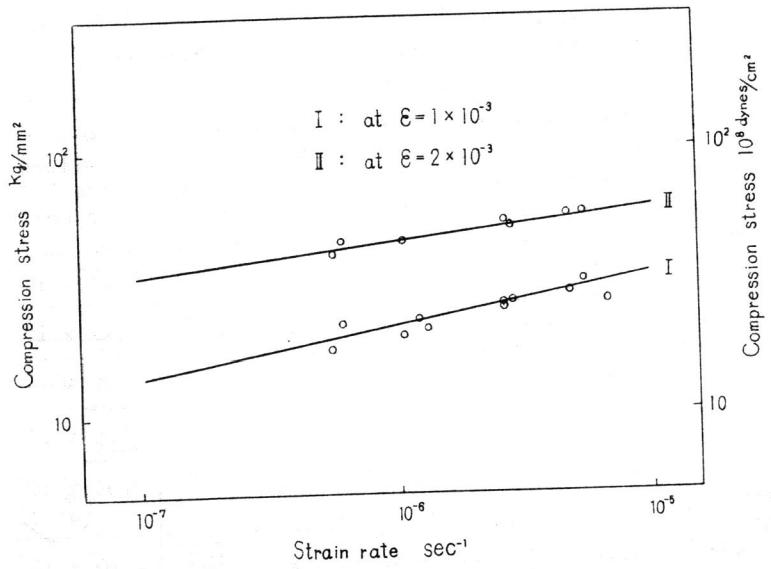

Fig. 2. Strain rate dependence of the flow stresses of sintered pellets at the strain of 1 x 10^{-3} and 2 x 10^{-3}

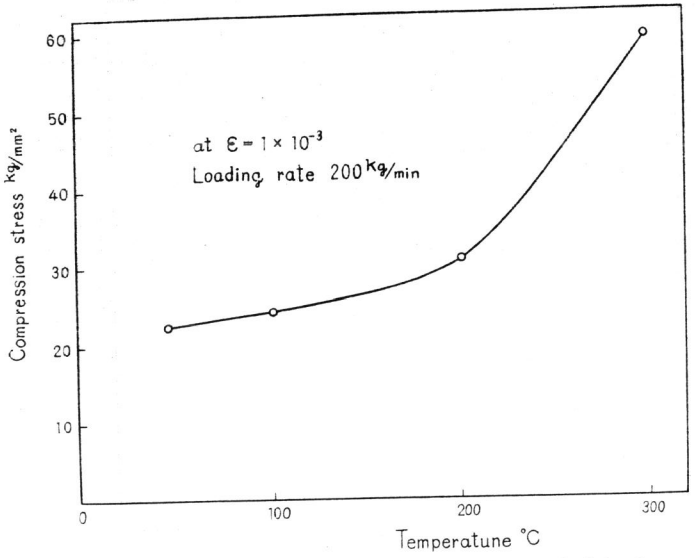

Fig. 3. Temperature dependence of the flow stresses of sintered pellets at the strain of 1 x 10^{-3}

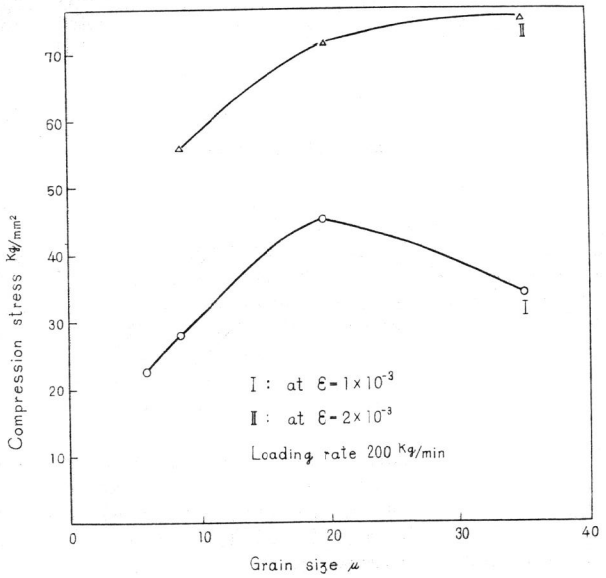

Fig. 4. Grain size dependence of the flow stresses of sintered pellets at the strain of 1 x 10^{-3} and 2 x 10^{-3}

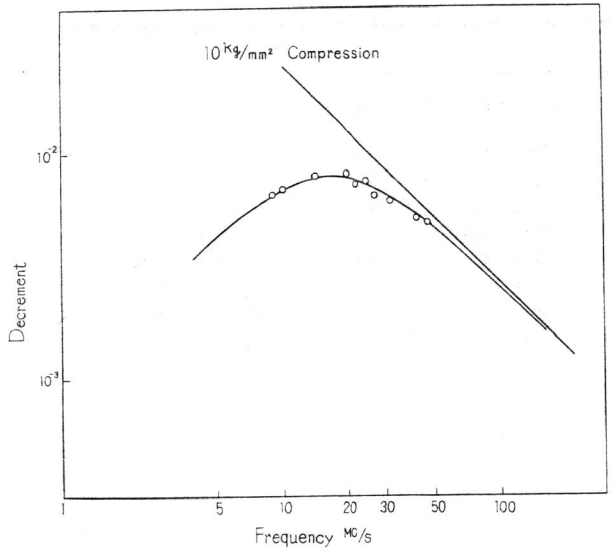

Fig. 5. Differential decrements against frequencies of fused single crystal. The full line shows the theoretical curve and the straight line shows the asymptote.

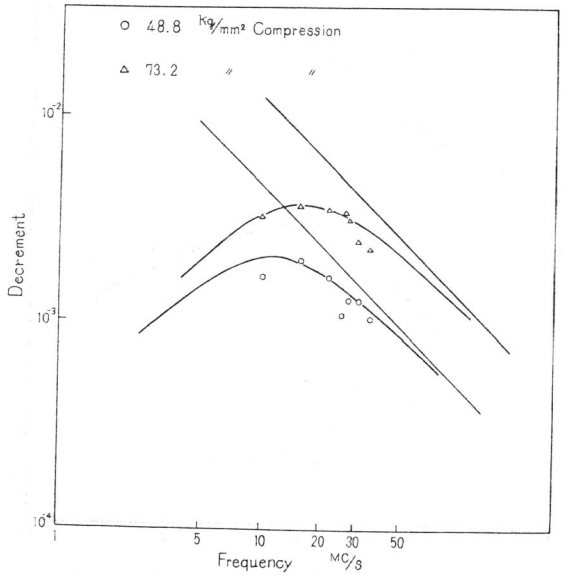

Fig. 6. Differential decrements against frequencies of sintered pellets. The full lines show the theoretical curves and the straight lines show the asymptotes.

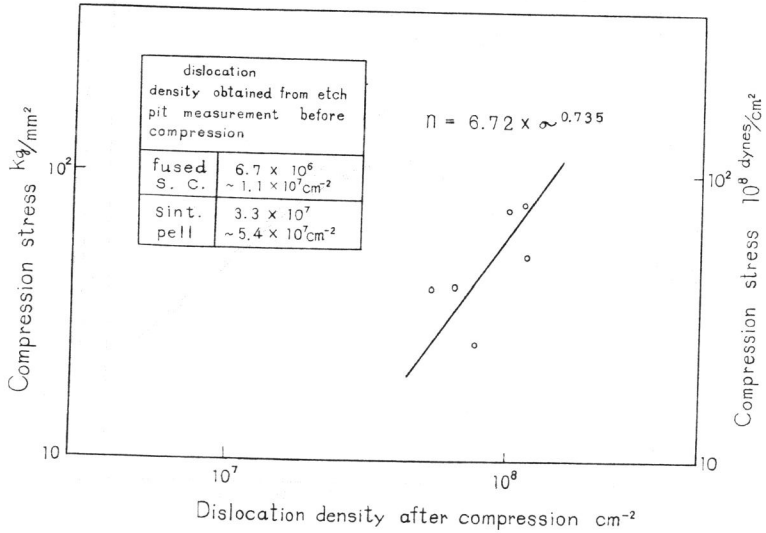

Fig. 7. Dislocation densities obtained from etch pit measurements before and after compression.